JACS
JOURNAL OF THE AMERICAN CHEMICAL SOCIETY
Communication
pubs.acs.org/JACS

Controlled Synthesis of ZrS_2 Monolayer and Few Layers on Hexagonal Boron Nitride

Mei Zhang,[†] Yiming Zhu,[†,‡] Xinsheng Wang,[†] Qingliang Feng,[†,§] Shanlin Qiao,[†] Wen Wen,[†] Yanfeng Chen,[†] Menghua Cui,[†] Jin Zhang,[§] Congzhong Cai,[‡] and Liming Xie*[,†]

[†]CAS Key Laboratory of Standardization and Measurement for Nanotechnology, National Center for Nanoscience and Technology, Beijing 100190, P. R. China

[‡]Department of Applied Physics, Chongqing University, Chongqing 401331, P. R. China

[§]Center for Nanochemistry, Beijing Science and Engineering Center for Nanocarbons, Beijing National Laboratory for Molecular Sciences, College of Chemistry and Molecular Engineering, Peking University, Beijing 100871, P. R. China

Supporting Information

ABSTRACT: Group IVB transition metal (Zr and Hf) dichalcogenide (TMD) monolayers can have higher carrier mobility and higher tunneling current density than group VIB (Mo and W) TMD monolayers. Here we report the synthesis of hexagonal ZrS_2 monolayer and few layers on hexagonal boron nitride (BN) using $ZrCl_4$ and S as precursors. The domain size of ZrS_2 hexagons is around 1−3 μm. The number of layers of ZrS_2 was controlled by tuning the evaporation temperature of $ZrCl_4$. The stacking angle between ZrS_2 and BN characterized by transmission electron microscopy shows a preferred stacking angle of near 0°. Field-effect transistors (FETs) fabricated on ZrS_2 flakes showed n-type transport behavior with an estimated mobility of 0.1−1.1 $cm^2\ V^{-1}\ s^{-1}$.

As a complementary material to zero-band-gap graphene, two-dimensional (2D) transition-metal dichalcogenides (TMDs) with sizable band gaps have attracted broad interest.[1−5] Whereas Group VIB TMD monolayers and few layers, such as MoX_2 and WX_2, (X = S, Se, Te), have been extensively studied, including their synthesis, optical properties, and electrical properties.[6−18] Group IVB TMD monolayers and few layers, such as ZrX_2 and HfX_2 (X = S, Se, Te), have rarely been studied but can have superior electrical properties.[19−28] The calculated room-temperature mobilities limited by acoustic phonons can be ∼1200 and ∼2300 $cm^2\ V^{-1}\ s^{-1}$ for ZrS_2 and $ZrSe_2$ monolayers, respectively, which are much higher than that of MoS_2 (∼400 $cm^2\ V^{-1}\ s^{-1}$).[24] Theoretical calculations also showed that ZrS_2-based and $ZrSe_2$-based tunneling field-effect transistors (TFETs) can have sheet current densities of up to 800 and 8000 $\mu A/\mu m$ (∼10^2 and ∼10^3 times higher than that of MoS_2), respectively, which are favored in low-power devices.[23] However, the synthesis of ZrX_2 (X = S, Se, Te) monolayers is challenging and has not been reported. The difficulties may arise from multiple Zr−X (X = S, Se) phases, including layered ZrX_2 as well as nonlayered Zr_3X_4 and ZrX_3.[29−33] Here, by using hexagonal boron nitride (BN) as a deposition template, we successfully synthesized high-quality ZrS_2 monolayer and few layers.

The strategy for the synthesis of ZrS_2 flakes is schematically illustrated in Figure 1a. Briefly, $ZrCl_4$ and S powders were placed in the upstream of the furnace at temperatures of ∼170 and 130 °C, respectively. The center of the furnace was heated to 950 °C. BN flakes on SiO_2/Si substrates were put in different positions in the downstream portion of the furnace, where the temperature was around 600−900 °C. The growth was done at a pressure of 0.6 Torr with an Ar and H_2 flow.

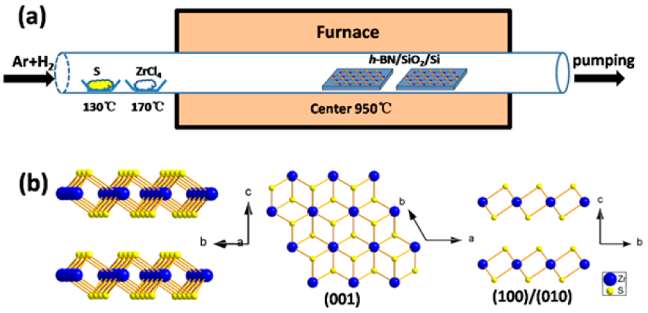

Figure 1. Illustrations of synthesis and crystal structure of layered ZrS_2. (a) Schematic of the low-pressure chemical vapor deposition (LPCVD) synthesis of ZrS_2 on a BN/SiO_2/Si substrate. (b) Chemical structure of 1T ZrS_2.

ZrS_2 crystals have the 1T structure, as shown in Figure 1b. The crystal constants are $a = b = 3.66$ Å and $c = 5.82$ Å.[33,34] Zr atoms are octahedrally coordinated by six sulfur atoms. In the S−Zr−S sandwich structure, the second S atomic layer is rotated by 60° with respect to the first S layer.

A typical scanning electron microscopy (SEM) image of ZrS_2 flakes on a BN substrate is shown in Figure 2a. ZrS_2 hexagonal flakes with sizes of 1−3 μm were selectively deposited only on BN flakes, while there were no ZrS_2 flakes on the bare SiO_2 regions. The reason could be that BN is an atomically flat substrate with a potentially lower nucleation rate, which is more favored in large-crystal growth. The low-magnification transmission electron microscopy (TEM) image in Figure 2b shows a ZrS_2 flake that was transferred onto a carbon grid. A

Received: April 13, 2015
Published: May 21, 2015

DOI: 10.1021/jacs.5b03807
J. Am. Chem. Soc. 2015, 137, 7051−7054

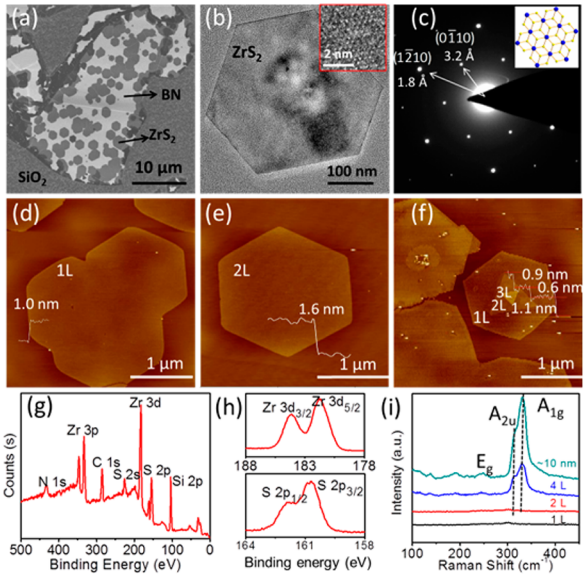

Figure 2. Characterizations of as-prepared ZrS_2 flakes. (a) SEM image of ZrS_2 deposited on BN/SiO_2/Si. (b) TEM and (inset) HRTEM images of hexagonal ZrS_2. (c) SAED pattern and (inset) schematic illustration of the atomic arrangement of the hexagonal ZrS_2 shown in (b). (d–f) AFM images of ZrS_2 monolayers and few layers. (g, h) XPS spectra of as-synthesized ZrS_2. (i) Raman spectra of as-synthesized ZrS_2 with different thicknesses.

honeycomb structure can be seen in the high-resolution TEM (HRTEM) image (Figure 2b inset). The selected-area electron diffraction (SAED) pattern corresponding to Figure 2b revealed hexagonal symmetry, with crystal plane distances of 3.2 and 1.8 Å corresponding to the {10$\bar{1}$0} and {11$\bar{2}$0} planes of ZrS_2.[35] The edge the ZrS_2 flake is oriented along the {11$\bar{2}$0} direction (Figure 2c inset). Atomic force microscopy (AFM) imaging was used to characterize the numbers of layers of as-synthesized ZrS_2 flakes (Figure 2d–f). The ZrS_2 monolayer showed a thickness of 1.0 nm (theoretical thickness of 0.58 nm[33,34]), while the ZrS_2 bilayer showed a height of ~1.6 nm.

Further, X-ray photoelectron spectroscopy (XPS) was used to characterize the chemical composition of the as-prepared ZrS_2 flakes (Figure 2g). The Zr $3d_{5/2}$ and Zr $3d_{3/2}$ peaks at 181.7 and 184.1 eV and the S $2p_{3/2}$ and S $2p_{1/2}$ peaks at 160.8 and 162.0 eV (Figure 2h) are consistent with the reported peak positions for ZrS_2.[32] Raman spectra of the ZrS_2 flakes are shown in Figure 2i. The E_g mode at 247 cm^{-1}, the A_{2u} mode at 314 cm^{-1}, and the A_{1g} mode at 331 cm^{-1} were observed from thick ZrS_2 flakes (four layer and 10 nm flakes).[36,37] No peaks were observed for the ZrS_2 monolayer and bilayers, possibly because of the weak signal and easy oxidation of the ZrS_2 monolayer and bilayer under laser irradiation in atmosphere.

The position of the BN/SiO_2/Si substrates (corresponding to different deposition temperatures) played an important role in the ZrS_2 deposition. The optimized deposition temperature was ~800 °C (Figure S1 in the Supporting Information (SI)), in which isolated large hexagonal ZrS_2 flakes were obtained. Higher deposition temperatures (i.e., substrates closer to the furnace center) gave thick inhomogeneous films. Lower deposition temperatures (i.e., substrates further from the furnace center) gave less dense and smaller ZrS_2 hexagons. Additionally, the total pressure and H_2 flow rate also affected the deposition (Figure S2). At lower total pressures, the ZrS_2 flakes were larger and thinner. At higher H_2 flow rates, the ZrS_2 flakes were thinner but more rounded. When the growth time was increased, the flakes became thicker and inhomogeneous (Figure S3).

The number of layers of ZrS_2 flakes can be controlled by tuning the evaporation temperature of $ZrCl_4$ (Figure 3). ZrS_2

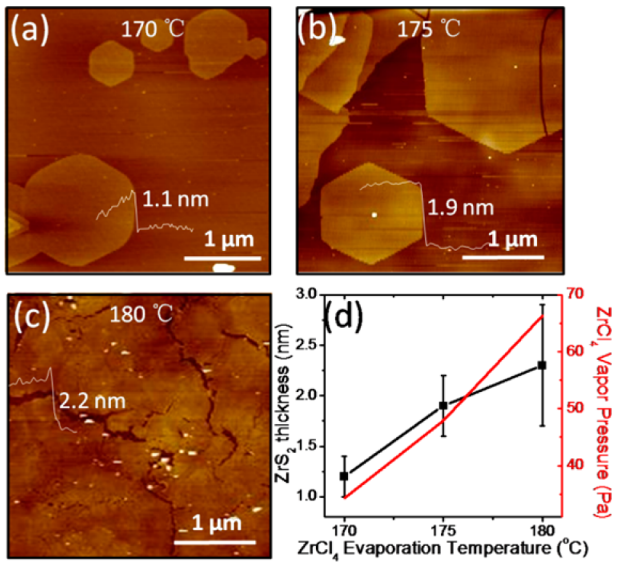

Figure 3. Controlling the layer number of ZrS_2 by tuning the $ZrCl_4$ evaporation temperature. (a-c) AFM analysis of ZrS_2 with different $ZrCl_4$ evaporation temperature: (a) 170 °C, (b) 175 °C, (c) 180 °C. (d) Vapor pressure and thickness with different $ZrCl_4$ evaporation.

flakes with average AFM heights of 1.2 ± 0.2 nm (mostly monolayer and a few bilayers), 1.9 ± 0.3 nm (bilayers and triple layers) and 2.2 ± 0.6 nm (two- to four-layer films) were obtained at $ZrCl_4$ evaporation temperatures of 170, 175, and 180 °C, respectively. The thickness of the as-prepared ZrS_2 flakes was correlated with the calculated temperature-dependent vapor pressure of $ZrCl_4$ (Figure 3d; also see the SI).

The van der Waals interactions as well as the lattice commensurability between ZrS_2 and BN should play key roles in the selective deposition of layered ZrS_2 on BN. In turn, investigation of the stacking angle between ZrS_2 flakes and the BN substrate can provide information on the angle-dependent ZrS_2–BN interaction. Figure 4a shows ZrS_2 hexagonal orientations on the same BN substrate. Since the BN substrate is a single-crystal domain, with the assumption that all of the ZrS_2 hexagons have the same edge orientation, the orientation distribution of the ZrS_2 hexagons on the same BN substrate can represent the relative stacking angles between ZrS_2 and BN. From SEM imaging, most of the ZrS_2 flakes are in one orientation (Figure 4f). To determine the absolute stacking angle between ZrS_2 and BN, TEM and SAED measurements were conducted. Figure 4b–d and Figure 4g–i show two typical results (1° and 8° stacking, respectively). In the SAED patterns, 3.2 and 1.8 Å correspond to the spacings of the ZrS_2 {10$\bar{1}$0} and {11$\bar{2}$0} planes and 2.2 and 1.2 Å to BN the {10$\bar{1}$0} and {11$\bar{2}$0} planes, respectively. The stacking angle between ZrS_2 and BN can be measured as the angle between the ZrS_2 ($\bar{1}$010) and BN ($\bar{1}$010) spots in the SAED pattern. HRTEM and fast Fourier transform (FFT) analysis also agreed with the stacking angles obtained from SAED. The schematic diagrams of the two different stacking structures shown in Figure 4e,j match well with the atom lines in Figure 4d,i. Counting of ~30

DOI: 10.1021/jacs.5b03807
J. Am. Chem. Soc. 2015, 137, 7051–7054

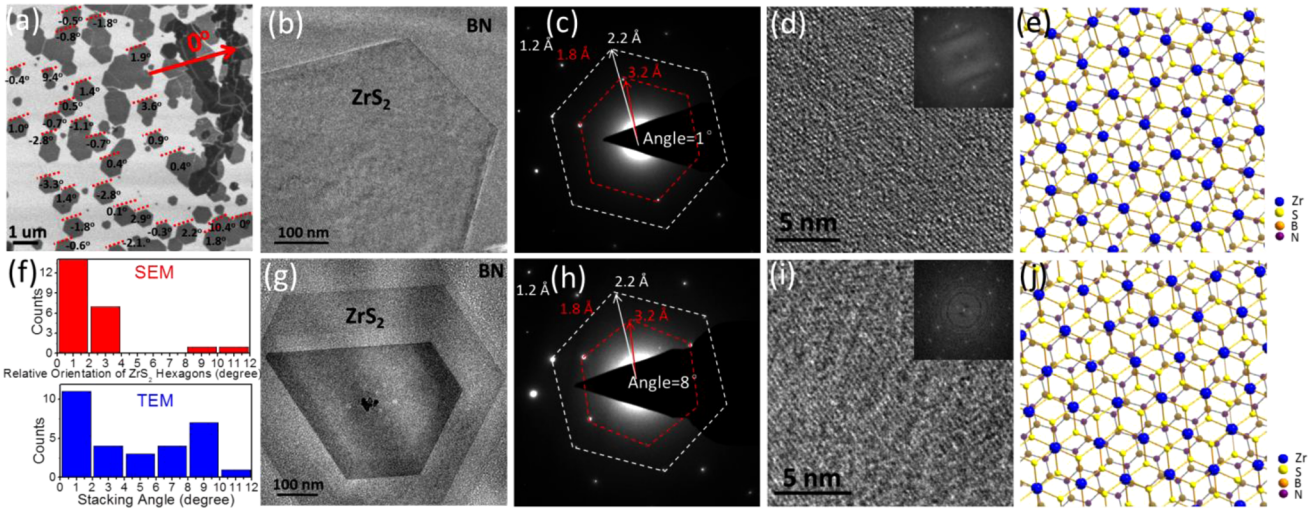

Figure 4. Characterization of stacking angles between ZrS_2 and BN. (a) SEM image of ZrS_2 hexagon angles on the same BN flake. The red arrow indicates an arbitrary reference direction. The stacking angles between ZrS_2 and BN are (b–e) 1° and (h–k) 8°, respectively. (b, g) Low-magnification TEM images of ZrS_2 on BN. (c, h) SAED patterns corresponding to (b) and (g), respectively. The spots in the red dashed hexagons indicate $\{10\bar{1}0\}$ planes of ZrS_2, and the spots in the white dashed hexagons indicate $\{10\bar{1}0\}$ planes of BN. (d, i) HRTEM image and (inset) FFT pattern. (e) Schematic diagram of the atomic arrangement consistent with (d). (j) Schematic diagram of the atomic arrangement consistent with (i). (f) Orientation distribution of ZrS_2 hexagons from SEM (red) and stacking angle distribution from TEM (blue).

different ZrS_2 flakes under TEM yielded the stacking angle distribution (Figure 4f), which revealed a preferred stacking angle of near 0°.

An FET was fabricated on ZrS_2 multilayers (Figure 5) using 50 nm Pt/5 nm Ti as contact electrodes. The channel length of

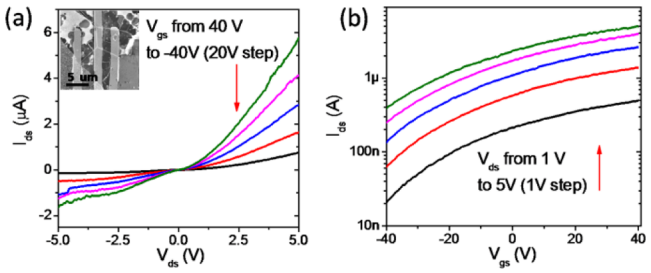

Figure 5. Electrical measurements on a ZrS_2 field-effect transistor. (a) Plot of the source–drain current (I_{ds}) vs the source–drain voltage (V_{ds}) with the gate voltage (V_{gs}) changing from 40 V to −40 V in steps of 20 V. The inset shows an SEM image of the device channel. (b) Plot of I_{ds} vs V_{gs} with V_{ds} changing from 1 to 5 V in steps of 1 V.

the FET was ∼2 μm (Figure 5a inset). The ZrS_2 devices exhibited n-type transport behavior (Figure 5b). The field-effect mobility μ_{FET} was estimated to be ∼1.1 $cm^2\ V^{-1}\ s^{-1}$, which is much lower than the theoretical mobility.[24] More effort is needed to engineer the contacts as well as the device structure.

In summary, we have presented an approach for synthesizing ZrS_2 atomic layers with a controlled number of layers by the LPCVD method on hexagonal BN. This method can also be used to synthesize $ZrSe_2$ monolayer and few layers (Figure S4). The obtained ZrS_2 layers exhibited a hexagonal shape with sizes of a few micrometers. The stacking angle between ZrS_2 and the BN substrate spans several degrees but is mostly near 0°. FET devices based on ZrS_2 flakes exhibited n-type transport behavior with an estimated mobility of ∼0.1–1.1 $cm^2\ V^{-1}\ s^{-1}$ (Figure S5). This simple and controllable approach opens up a new way to produce highly crystalline ZrS_2 and $ZrSe_2$ atomic layers and the potential for HfX_2 (X = S, Se), which are promising materials for nanoelectronics.

■ ASSOCIATED CONTENT

Supporting Information

Experimental details; effects of deposition temperature, Ar/H_2 flow rate, and growth time on ZrS_2 synthesis; relationship between $ZrCl_4$ evaporation temperature and vapor pressure; estimation of ZrS_2 mobility; characterization of as-synthesized $ZrSe_2$ monolayer and few layers; and more electrical measurements on ZrS_2 FETs. The Supporting Information is available free of charge on the ACS Publications website at DOI: 10.1021/jacs.5b03807.

■ AUTHOR INFORMATION

Corresponding Author

*xielm@nanoctr.cn

Notes

The authors declare no competing financial interest.

■ ACKNOWLEDGMENTS

L.X. acknowledges support from the National Natural Science Foundation of China (NNSFC) (21373066 and 11304052), the Beijing Nova Program (2015B049), and the China Postdoctoral Science Foundation (2013M540900). J.Z. acknowledges support from the NNSFC (21233001, 21129001, 51272006, and 51121091).

■ REFERENCES

(1) Wang, Q. H.; Kalantar-Zadeh, K.; Kis, A.; Coleman, J. N.; Strano, M. S. *Nat. Nanotechnol.* **2012**, *7*, 699.
(2) Schwierz, F. *Nat. Nanotechnol.* **2010**, *5*, 487.
(3) Chhowalla, M.; Shin, H. S.; Eda, G.; Li, L. J.; Loh, K. P.; Zhang, H. *Nat. Chem.* **2013**, *5*, 263.
(4) Eda, G.; Maier, S. A. *ACS Nano* **2013**, *7*, 5660.
(5) Xie, L.; Wang, H.; Jin, C.; Wang, X.; Jiao, L.; Suenaga, K.; Dai, H. *J. Am. Chem. Soc.* **2011**, *133*, 10394.
(6) Yu, Y.; Li, C.; Liu, Y.; Su, L.; Zhang, Y.; Cao, L. *Sci. Rep.* **2013**, *3*, 1866.

DOI: 10.1021/jacs.5b03807
J. Am. Chem. Soc. 2015, 137, 7051–7054

(7) Najmaei, S.; Liu, Z.; Zhou, W.; Zou, X.; Shi, G.; Lei, S.; Yakobson, B. I.; Idrobo, J. C.; Ajayan, P. M.; Lou, J. *Nat. Mater.* **2013**, *12*, 754.
(8) Yu, J. H.; Lee, H. R.; Hong, S. S.; Kong, D.; Lee, H. W.; Wang, H.; Xiong, F.; Wang, S.; Cui, Y. *Nano Lett.* **2015**, *15*, 1031.
(9) Ruppert, C.; Aslan, O. B.; Heinz, T. F. *Nano Lett.* **2014**, *14*, 6231.
(10) Liu, W.; Kang, J.; Sarkar, D.; Khatami, Y.; Jena, D.; Banerjee, K. *Nano Lett.* **2013**, *13*, 1983.
(11) Jo, S.; Ubrig, N.; Berger, H.; Kuzmenko, A. B.; Morpurgo, A. F. *Nano Lett.* **2014**, *14*, 2019.
(12) Wang, X.; Feng, H.; Wu, Y.; Jiao, L. *J. Am. Chem. Soc.* **2013**, *135*, 5304.
(13) Huang, X.; Zeng, Z.; Zhang, H. *Chem. Soc. Rev.* **2013**, *42*, 1934.
(14) Feng, Q.; Zhu, Y.; Hong, J.; Zhang, M.; Duan, W.; Mao, N.; Wu, J.; Xu, H.; Dong, F.; Lin, F.; Jin, C.; Wang, C.; Zhang, J.; Xie, L. *Adv. Mater.* **2014**, *26*, 2648.
(15) Lee, Y. H.; Zhang, X. Q.; Zhang, W.; Chang, M. T.; Lin, C. T.; Chang, K. D.; Yu, Y. C.; Wang, J. T.; Chang, C. S.; Li, L. J.; Lin, T. W. *Adv. Mater.* **2012**, *24*, 2320.
(16) Zhang, M.; Wu, J.; Zhu, Y.; Dumcenco, D. O.; Hong, J.; Mao, N.; Deng, S.; Chen, Y.; Yang, Y.; Jin, C.; Chaki, S. H.; Huang, Y. S.; Zhang, J.; Xie, L. *ACS Nano* **2014**, *8*, 7130.
(17) Pradhan, N. R.; Rhodes, D.; Feng, S.; Xin, Y.; Memaran, S.; Moon, B. H.; Terrones, H.; Terrones, M.; Balicas, L. *ACS Nano* **2014**, *8*, 5911.
(18) Chen, Y.; Xi, J.; Dumcenco, D. O.; Liu, Z.; Suenaga, K.; Wang, D.; Shuai, Z.; Huang, Y. S.; Xie, L. *ACS Nano* **2013**, *7*, 4610.
(19) Li, Y.; Kang, J.; Li, J. B. *RSC Adv.* **2014**, *4*, 7396.
(20) Lucovsky, G.; White, R. M.; Benda, J. A.; Revelli, J. F. *Phys. Rev. B* **1973**, *7*, 3859.
(21) Kreis, C.; Werth, S.; Adelung, R.; Kipp, L.; Skibowski, M.; Krasovskii, E. E.; Schattke, W. *Phys. Rev. B* **2003**, *68*, No. 235331.
(22) Gaiser, C.; Zandt, T.; Krapf, A.; Serverin, R.; Janowitz, C.; Manzke, R. *Phys. Rev. B* **2004**, *69*, No. 075205.
(23) Fiori, G.; Bonaccorso, F.; Iannaccone, G.; Palacios, T.; Neumaier, D.; Seabaugh, A.; Banerjee, S. K.; Colombo, L. *Nat. Nanotechnol.* **2014**, *9*, 768.
(24) Zhang, W. X.; Huang, Z. S.; Zhang, W. L.; Li, Y. R. *Nano Res.* **2014**, *7*, 1731.
(25) Jiang, H. *J. Chem. Phys.* **2011**, *134*, No. 204705.
(26) Tributsch, H. *Faraday Discuss.* **1980**, *70*, 189.
(27) Gong, C.; Zhang, H. J.; Wang, W. H.; Colombo, L.; Wallace, R. M.; Cho, K. J. *Appl. Phys. Lett.* **2013**, *103*, No. 053513.
(28) Li, L.; Fang, X.; Zhai, T.; Liao, M.; Gautam, U. K.; Wu, X.; Koide, Y.; Bando, Y.; Golberg, D. *Adv. Mater.* **2010**, *22*, 4151.
(29) Greenaway, D. L.; Nitsche, R. *J. Phys. Chem. Solids* **1965**, *26*, 1445.
(30) Learfield, A. *J. Am. Chem. Soc.* **1958**, *80*, 6511.
(31) Moustafa, M.; Zandt, T.; Janowitz, C.; Manzke, R. *Phys. Rev. B* **2009**, *80*, No. 035206.
(32) Whitehouse, C. R.; rimmington, H. P. R.; Balchi, A. A. *Phys. Status Solidi A* **1973**, *18*, 623.
(33) Patel, S. G.; Arora, S. K.; Agarwal, M. K. *Bull. Mater. Sci.* **1998**, *21*, 297.
(34) Al-Alamy, F. A. S.; Balchin, A. A.; White, M. *J. Mater. Sci.* **1977**, *12*, 2037.
(35) Jang, J. T.; Jeong, S.; Seo, J. W.; Kim, M. C.; Sim, E.; Oh, Y.; Nam, S.; Park, B.; Cheon, J. *J. Am. Chem. Soc.* **2011**, *133*, 7636.
(36) Roubi, L.; Carlone, C. *Phys. Rev. B* **1988**, *37*, 6808.
(37) Stacy, A. M.; Hodul, D. T. *J. Phys. Chem. Solids* **1985**, *46*, 405.

DOI: 10.1021/jacs.5b03807
J. Am. Chem. Soc. 2015, 137, 7051−7054